Anti-biofilm super-hydrophilic gel sensor for saliva glucose monitoring

Tingjun Chen [a], Jing Pang [b], Xinchuan Liu [a], Na Chen [a,c], Chenchen Wu [a,c], Yu Duan [a], Xuefu You [b], Qian Dou [a,c,*], Chao Yuan [d,*], Yanxiang Wang [b,*] and Qing Dai [a,c]

[a] CAS Key Laboratory of Nanophotonic Materials and Devices, CAS Key Laboratory of Standardization and Measurement for Nanotechnology, CAS Center for Excellence in Nanoscience, National Center for Nanoscience and Technology, Beijing 100190, China

[b] Beijing Key Laboratory of Antimicrobial Agents, Institute of Medicinal Biotechnology, Chinese Academy of Medical Sciences and Peking Union Medical College, Beijing 100050, China

[c] Center of Materials Science and Optoelectronics Engineering, University of Chinese Academy of Sciences, Beijing 100049, China

[d] Department of Preventive Dentistry, Peking University School and Hospital of Stomatology, National Center for Stomatology, National Clinical Research Center for Oral Diseases, National Engineering Research Center of Oral Biomaterials and Digital Medical Devices

Abstract

Accurate detection of saliva glucose level has important clinical significance for the diagnosis of diabetes and oral diseases. However, overcoming the decrease in sensor sensitivity caused by bacterial adhesion remains challenging for antibacterial materials due to the intricate bacterial environment present in the oral cavity. The excellent self-cleaning capabilities of super-hydrophilic materials make them one of the top choices. To address the limitations of conventional artificially synthesized super-hydrophilic materials, a Spin coating-Plasma treatment-Coprecipitation treatment (SPC) strategy was employed to develop a super-hydrophilic gel saliva glucose sensor. Surface-initiated polymerization was

used to form phenylboric acid hydrogels for glucose binding, spin-coated transition layer was applied to protect the hydrogel, and plasma treatment and co-precipitation methods were utilized to create a super-hydrophilic surface on the hydrogel, enabling antibacterial action. The results show that the super-hydrophilic gel sensor reduced bacterial adhesion of the five oral pathogenic bacteria by over 95%, and inhibited the biofilm formation of *Streptococcus pneumoniae* and *Streptococcus mitis* by 95.7% and 96.7%, respectively. Additionally, the detection limit of the sensor reached 3.04 mg/L, fully satisfying the requirements for saliva glucose detection. Overall, the successful construction of the super-hydrophilic gel sensor can be used for wearable oral monitoring devices, particularly in the context of managing and monitoring health conditions.

Keywords: saliva glucose, sensor sensitivity, bacterial adhesion, super-hydrophilic gel sensor, wearable oral monitoring

Introduction

Saliva glucose exhibits a strong correlation with blood glucose levels, making it an ideal candidate for non-invasive blood glucose monitoring [1-4]. Meanwhile, the rise of saliva glucose would lead to the growth of oral pathogens, leading to various oral diseases [5-7]. Consequently, real-time monitoring of saliva glucose concentration holds significant clinical importance. However, the challenge of bacterial adhesion poses a major obstacle for oral wearable sensors. Indeed, the human mouth harbors a vast

and intricate bacterial system, consisting of approximately 700 bacterial species [8], which can potentially colonize the surface of these sensors and form biofilms, thereby diminishing the sensitivity and longevity of implanted sensors [9-11]. Bacterial biofilm formation follows a multi-step dynamic process (Figure 1) [12-14]. I) Initially, bacteria make contact with the material's surface, resulting in reversible bacterial adhesion. II) Subsequently, genes associated with biofilm formation are activated, leading to irreversible adherence of bacteria to the material's surface. III) As the biofilm matures, the bacteria organize into a highly structured microcolony. IV) Bacteria shed or are released from mature biofilms, reverting to a planktonic state, and have the potential to form new biofilms. Thus, during saliva glucose detection, a large number of bacteria will attach to the surface of the sensor to form biofilms, affecting the accuracy and reliability of the sensor [15-17].

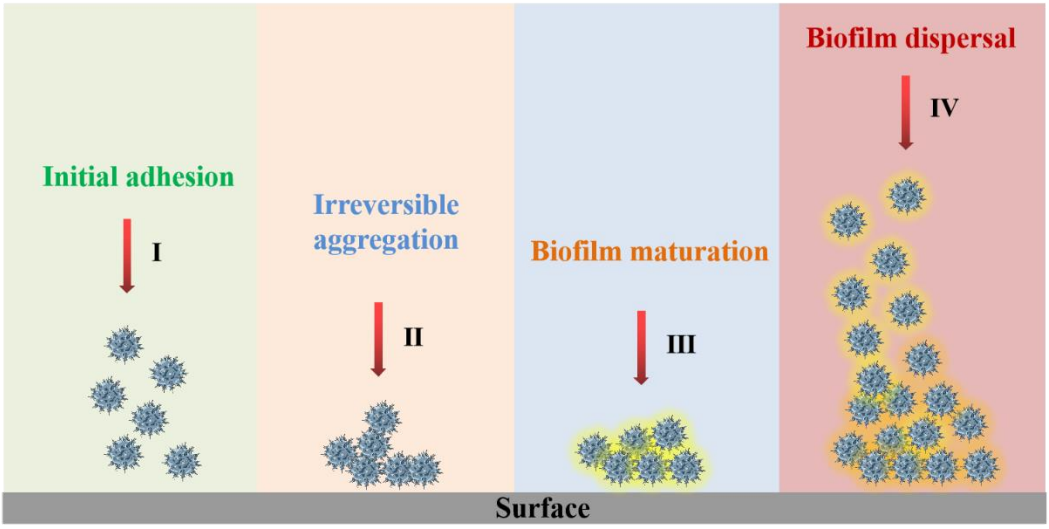

Figure 1. The process by which bacteria form biofilms. I) initial adhesion, II) irreversible aggregation, III) biofilm maturation, and IV) biofilm dispersal.

Research shows that materials' degree of hydration is positively correlated with their antifouling and anti-bacterial adhesion capacity [18, 19]. Therefore, super-hydrophilic materials become the preferred choice for anti-pollution materials. Indeed, by the formation of a hydration layer on the material surface, the super-hydrophilic coating prevents bacteria from entering in contact with the material’s surface and can remove surface bacteria under the scouring of water, thereby achieving a self-cleaning effect [20-22]. There are generally two approaches to achieving super-hydrophilic surfaces: one involves constructing rough structures on hydrophilic surfaces [23, 24]. Li *et al.* utilized a hydrothermal synthesis method to create microscale rough structures on the surface of aluminum and its alloys, resulting in a super-hydrophilic surface [25]. The other approach involves introducing hydrophilic functional groups onto the surface [26, 27]. An *et al.* grafted hyperbranched polyglycerol onto a polyamide thin film composite layer, resulting in the formation of a super-hydrophilic surface with excellent anti-fouling properties [28]. However, the incorporation of micro-nano rough structures in the material preparation process introduces significant complexity and time consumption. Moreover, this approach may limit the stability and durability of nanostructures. Additionally, directly grafting hydrophilic functional groups to the material surface can lead to issues with grafting density and homogeneity, leading to an uneven hydrophilic surface.

Therefore constructing a super-hydrophilic coating on the surface of a sensor still poses higher demands on the material's stability.

In this work, a sensor with a super-hydrophilic surface has been successfully constructed. Subsequently, we conducted the following studies: i) explore the bacterial adhesion-preventing ability of the super-hydrophilic gel sensor to oral bacteria, ii) verify the biofilm formation resistant ability of the sensor to the predominant bacteria at high saliva glucose levels, iii) evaluate the accuracy of the sensor for the saliva glucose determination. The results demonstrate that the super-hydrophilic hydrogel sensor exhibits an antibacterial adhesion rate increase of over 95% against five oral pathogenic bacteria and effectively inhibits the formation of bacterial biofilms. Moreover, the detection limit of this sensor reaches 3.04 mg/L, it fully meets the needs of salivary glucose detection.

Experimental section

Reagents and instruments

3-Aminopropyltriethoxysilane (98%) and polyethyleneimine (PEI，99%, M_w 1800) were purchased from Alfa Aesar Chemicals Co., Ltd. (3-Methacrylamidophenyl) boronic acid (PBA，99.92%, Ark Pharm, Inc.), N,N-Methylenebisacrylamide (BIS, 98%, Sinopharm Chemical Reagent Co. Ltd.), acrylamide (AM, 99.0%), tannic acid (TA), polyvinylpyrrolidone (PVP) were purchased from Macklin Biochemical Co., Ltd. 2,2-Dimethoxy-1,2-diphenylethanone (DMPA, 98.0%, TCI

Development Co., Ltd.), Carboxylated nanofiber cellulose (CNF-C, Qihong Technology Co., Ltd.), polyethyleneimine (bPEI, M_w 25000), Crystal violet was purchased from Innochem. Glucose, N,N-dimethylformamide, and maleic anhydride are all pure analytical reagents. Brain Heart Infusion (BHI) broth and agar used for bacterial cultures were purchased from Becton, Dickinson and Company. Filmtracer™ SYPRO® Ruby Biofilm Matrix Stain was purchased from Thermo Fisher Scientific Inc.

Saliva glucose level and anti-protein properties were tested by Quartz crystal microbalance (QCM 200, Stanford Research Systems). Reactive Ion Etching (ETCHLAB 200) was used for plasma treatment. The morphologies of the sensor surface were investigated using Scanning Electron Microscope (SEM, SU-8200). Hydrophilicity was measured using a fully automatic contact angle measuring instrument (DSA-100). X-ray Photoelectron Spectroscopy (XPS, ESCALAB250Xi) was used to determine the elemental composition of sensor surfaces. The external force applied during the sensor coating formation was achieved through a lab-built pressure film machine. Ultraviolet polymerization was performed using a UV lamp (wavelength λ = 365 nm and maximum power = 3 W). Spin coating of films was performed using a Spin-coater (KW-4B, Beijing SETCAS Electronics Co., Ltd.). The stained biofilm matrix imaging was performed on an IVIS® Spectrum in Vivo Imaging System (IVIS,

PerkinElmer Inc.).

Surface modification of the QCM electrode

The preprocessing of chips was performed as described in our previous work. In short, the QCM chips were placed in a piranha solution (H_2SO_4 (98% w/w) and H_2O_2 (30% w/w) in a volume ratio of 7:3 and were ultrasonicated for 10 min, then rinsed with distilled water and dried with N_2. Subsequently, the chips were ultrasonicated in acetone, ethanol, then distilled water for 10 min respectively, then dried with N_2. The treated chips were placed in a mixture of 3-aminopropyl triethoxysilane and toluene (v/v 1:10) for 12 h, rinsed with ethanol and dried with N_2. Finally, the dried chips were immersed in a mixture of maleic anhydride (25 mL) and N,N-dimethylformamide (500 mg) for 12 h, rinsed with ethanol and dried with N_2 for further modification.

Preparation of PBA hydrogel (HPBA)

First, the surface of the chip was modified using surface-initiated polymerization. PBA (17.2 mg), BIS (1.54 mg), AM (27.7 mg), and DMPA (2.56 mg) were added into 100 μL of DMSO to form the prepolymer. Then, 30 μL of the prepolymer was deposited on the processed chip under pressure to form a thin film with uniform thickness [29]. Finally, HPBA was obtained after placing the chips under ultraviolet light (λ=365 nm) for 1 h. Then, the chips were rinsed with distilled water and dried with N_2 for future modification. The HPBA containing glucose-capturing unit PBA,

AM, and BIS was used to construct the hydrogel framework, and as a free radical photoinitiator, DMPA was used to initiate the polymerization and the crosslinking of AM and BIS.

Preparation of CNF-C@bPEI/HPBA

A transition layer was modified on HPBA using spin coating. For this, CNF-C (2 g) was added into 40 mL of distilled water containing EDC (80 mg) and NHS (120 mg) and was allowed to react for 15 min. Next, PEI (2 g) was added and the mixture was stirred overnight with a magnetic stirrer. The obtained white floccules were centrifuged at high speed (10000 rpm, 10 min), and the supernatant was removed. The pellet was then redispersed in 1 mL of ethanol to obtain the spin-coating solution. Finally, 50 μL of the spin coating solution was used to prepare CNF-C@bPEI/ HPBA using spin coating (low-speed: 500 rpm, 5 s, high-speed: 3000 rpm, 30 s), then the chips were rinsed with distilled water and dried with N_2.

Preparation of Plasma-treated CNF-C@bPEI/HPBA

Plasma surface treatment technology can easily and effectively change the chemical composition and rough structure of the surfaces of materials. Plasma-treated CNF-C@bPEI/HPBA was obtained after treatment with O_2 plasma (O_2 flow rate: 20 sccm, time: 5 min, power: 200 W). The plasma-treated chips were then rinsed with distilled water and dried with N_2. This step significantly increases the free energy of the Plasma-treated CNF-C@bPEI/HPBA surface and reduces the surface wetting angle, thus

achieving the super-wettability state.

Preparation of Coprecipitation-treated CNF-C@bPEI/HPBA

Due to the high energy of polar groups, the hydrophobic polymer chain can embed these groups on the inside through rearrangement, resulting in a "hydrophobic recovery" phenomenon. Therefore, we prolonged the super-hydrophilic aging through mild coprecipitation treatment. TA (20 mg), PEI (5 mg), and PVP (50 mg) were dissolved in 30 mL of distilled water by ultrasonication to obtain the coprecipitation solution. Coprecipitation-treated CNF-C@bPEI/HPBA chips were obtained by placing Plasma-treated CNF-C@bPEI/HPBA chips face up in the coprecipitation solution for 12 h. Finally, the chips were rinsed with distilled water and dried with N_2 for subsequent testing.

QCM measurements

Coprecipitation-treated CNF-C@bPEI/HPBA were placed in the QCM flow cell. Phosphate buffer solution (PBS) (0.1 mol/L) was continuously pumped into the flow cell at an appropriate flow rate under the action of a peristaltic pump, and the change of the chip frequency (ΔF) was monitored in real-time by the QCM data acquisition software. When ΔF was stable, we investigated the sensitivity of glucose detection and antifouling performance.

Saliva samples

The collection of saliva samples was supported by the "Early identification,

early diagnosis, and cutting point of diabetes risk factors" program (2016YFC1305700). Saliva samples were collected from ordinary urban and rural residents in Yancheng, Jiangsu Province, China, who were between 18 and 65 years old and had no history of mental illness. Informed consent was obtained from all participants and experiments were approved by the Medical ethics committee of Jiangsu Provincial Center for Disease Control and Prevention (JSJK2017-B003-02), China.

Saliva collection and processing

Five males and five females between the ages of 20 and 40, who were restricted to glucose drinks 1 h before sample collection were selected for the study. Subjects drank 200 mL of water 30 min before collecting the saliva sample.

A saliva collector was used to collect non-irritating saliva. During sample collection, subjects relaxed, sat upright, tilted their heads slightly, and spat saliva naturally into the sterile disposable centrifuge tube. A total of 15 mL sample was collected from each subject.

The collected saliva samples were divided into 6 groups for each subject. Different concentrations of glucose were added to each group’s samples (0 mg/L, 50 mg/L, or 100 mg/L glucose, two groups for each concentration). Then, the saliva samples with the same concentration were stored at room temperature for 1 h or 2 h. The processed saliva samples were stored at −80°C until the oral flora analysis. The specific operation flow chat is

described in Figure S1.

Antibacterial measurements

All bacterial strains used in this study were obtained from the Collection Center of Pathogen Microorganisms of Chinese Academy of Medical Sciences (CAMS-CCPM-A), China. Widely distributed bacteria in saliva and daily environment, *Staphylococcus epidermidis* (*S. epidermidis*) ATCC 12228, *Streptococcus mutans* (*S. mutans*) ATCC 25715, *Streptococcus pneumoniae* (*S. pneumoniae*) ATCC 51916, *Streptococcus mitis* (*S. mitis*) ATCC 49456, *Streptococcus oralis* (*S. oralis*) ATCC 35037 were chosen for the adhesion experiments and were stored at −80°C. These bacteria were incubated by streaking on brain heart infusion (BHI) agar plates to make fresh overnight cultures. Then, one colony of each strain was inoculated into 10 mL of BHI broth and incubated for 24 h at 37°C except for *S. mutans* which required a longer incubation time of 48 h. *S. mitis*, *S. pneumoniae*, and *S. oralis* were inoculated anaerobically. Bacteria were then harvested by centrifugation (2400 *g*) for 10 min, washed twice in sterile PBS, and their concentration was adjusted to 1×10^7 CFU/mL in sterile PBS for the adhesion experiments.

The different surfaces were placed in 2 mL bacterial suspension in 6-well cell culture plates and were incubated for 3 h at 37°C. After incubation, samples were picked up with sterile forceps, mildly rinsed with sterile PBS to remove the loosely adherent bacteria, and soaked in 2 mL of sterile PBS

in new 6-well cell culture plates. To quantify viable adherent bacteria, the plates were subjected to a 30 s sonication, and 10 μL serially diluted samples were drop-plated on BHI agar plates in triplicates. The plates were incubated at 37°C for 24 or 48 h and the colony-forming units (CFU) were counted. The results were expressed as CFU/mL.

To investigate the bacterial cell morphology on different surfaces, one sample from each group was fixed with 2.5 wt% glutaraldehyde for 24 h. Then, they were passed through an ethanol gradient for dehydration, dried, coated with gold, and observed using SEM.

Biofilm adhesion measurements

S. mitis, S. pneumoniae, and *S. oralis* were cultured anaerobically overnight at 37 °C. The different sensors were immersed in 2 mL of 1:100 diluted overnight inoculums in 6-well cell culture plates to form biofilms for 24 h. Samples were then mildly washed with PBS 3 times to remove planktonic bacteria for the subsequent study.

Drop plate method was used for determining viable counts of bacteria in biofilm as described above. For fluorescence staining, the biofilm matrix was quantified by staining with Filmtracer SYPRO Ruby Biofilm Matrix Stain. In the crystal violet staining, biofilms were fixed at 60 °C, then 1 mL of 0.06% crystal violet was added to each well, stained for 5 min, and crystal violet was removed by repeated washing with water.

Results and Discussion

Synthesis of the super-hydrophilic gel sensor

The SPC strategy was employed to design and construct a super-hydrophilic coating on the PBA hydrogel for preventing biological contamination on the sensor surface and ensuring accurate glucose detection in saliva. The specific design steps are outlined as follows (Figure 2a): i) the polymerization reaction was initiated by ultraviolet irradiation to form a glucose-responsive hydrogel on the chips (HPBA). ii) spin-coating a transition layer on the surface of HPBA (CNF-C@bPEI/HPBA) to shield it from direct bombardment during plasma treatment, iii) the plasma treatment etches the material, introduces hydrophilic groups on the surface, and form a micro-nano rough structure, resulting in a super-hydrophilic state (Plasma-treated CNF-C@bPEI/HPBA), iv) delaying and improving the "hydrophobicity recovery" of super-hydrophilic materials through co-precipitation (Coprecipitation-treated CNF-C@bPEI/HPBA), thus further enhancing the hydrophilic properties. The introduction of the transition layer not only enhances the hydrophilic functional groups and permeability of the surface but also protects the stability of the underlying hydrogel. Plasma treatment addresses the issue of non-uniform hydrophilic functional group distribution while preserving the intrinsic substrate properties. Co-precipitation method further enhances the stability of the super-hydrophilic coating, resulting in a 10-fold improvement in its super-hydrophilic stability. For a more detailed description of the construction

process and characterization results of the superhydrophilic hydrogel sensor, please refer to the Supplementary Material. (Table S1, Figure S2-6). Based on this, when the super-hydrophilic gel sensor detects saliva glucose, the hydration on the sensor surface can prevent bacterial contact and biofilm formation, and ultimately safeguards the sensor from biocontamination.

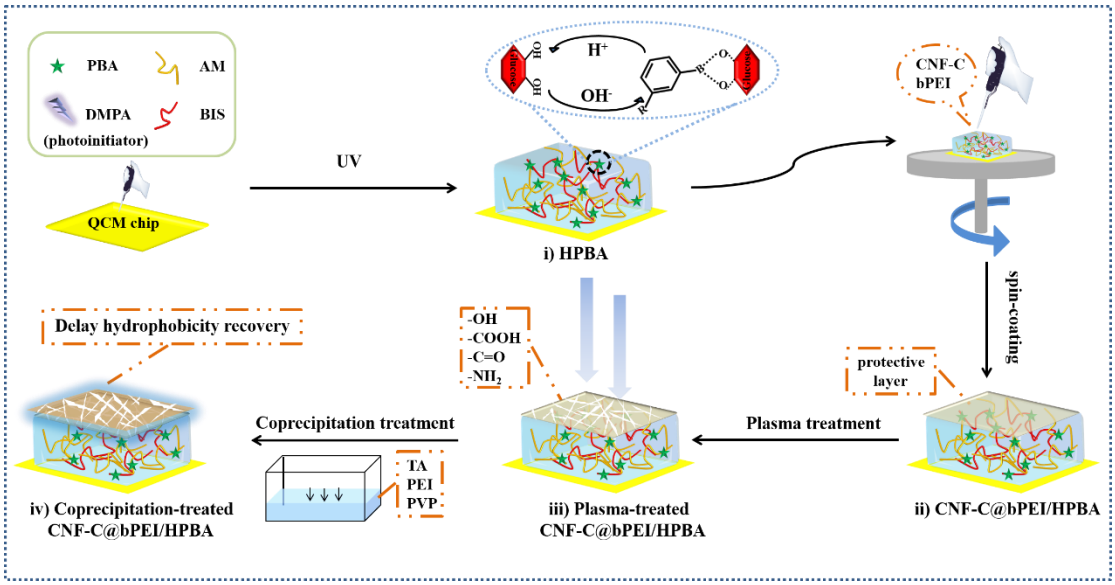

Figure 2. The schematic illustration of the synthesis of super-hydrophilic gel sensor.

Bacterial adhesion-preventing properties of super-hydrophilic gel sensor

To compare the effect of the different modifications, antibacterial experiments were performed on the different modification stages of the sensor (Figure 3a). The relatively high abundant *Staphylococcus* and *Streptococcus* in the oral cavity were taken as examples to assess the impact of bacteria on different surface sensors (Figure 3b). The results showed that the super-hydrophilic coating displayed a significant anti-adhesion effect on all five bacterial strains when compared to the hydrogel

coating. The anti-adhesion efficacies for *S. epidermidis*, *S. mutans*, *S. pneumoniae*, *S. mitis* and *S. oralis* were increased by 96.3 ± 0.30%, 98.4 ± 0.31%, 96. 8± 0.28%, 99.9 ± 0.02% and 95.2 ± 1.18%, respectively (Table S2, Figure S7).

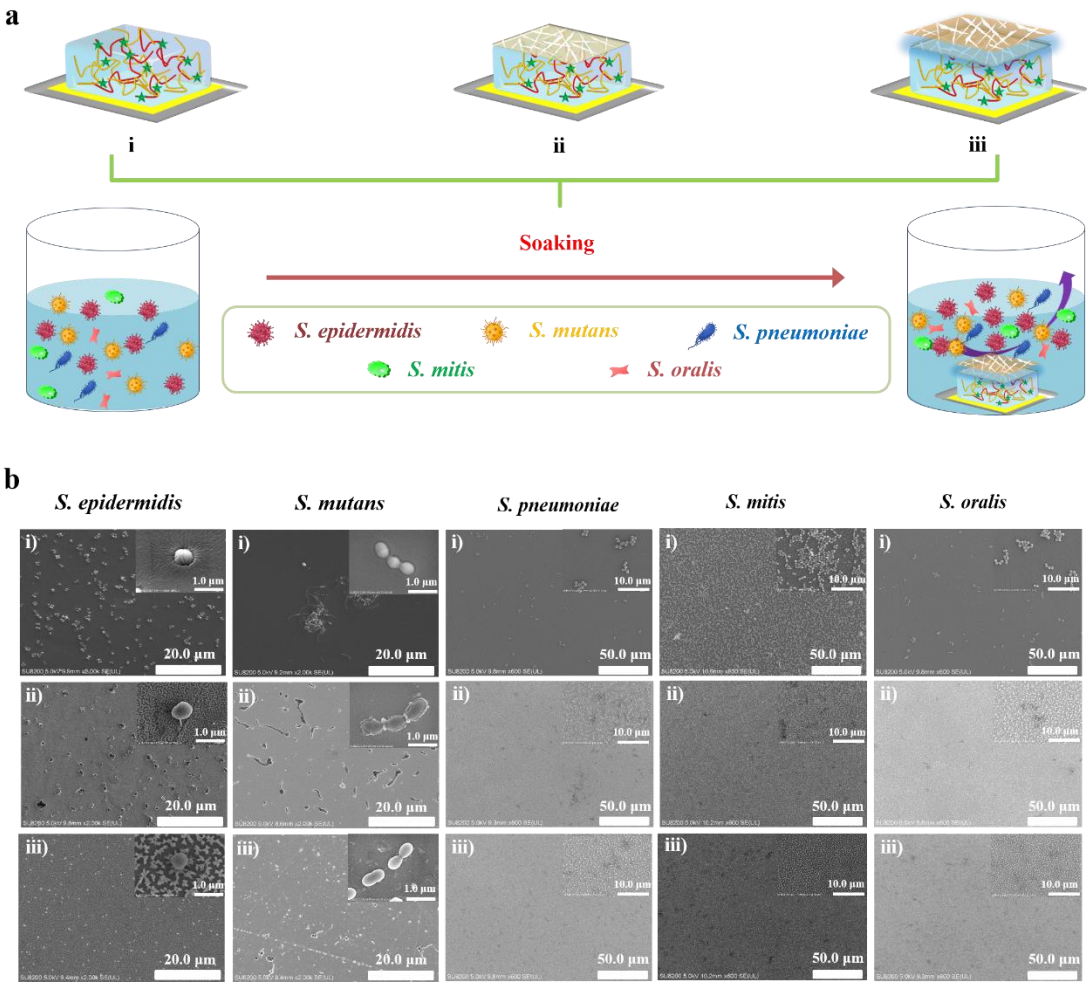

Figure 3. a) Effects of bacteria on different modification sensors: i) HPBA, ii) Plasma-treated CNF-C@bPEI/HPBA, iii) Coprecipitation-treated CNF-C@bPEI/HPBA. b) SEM images of bacterial adsorption on sensors. (i) HPBA, (ii) Plasma-treated CNF-C@bPEI/HPBA, (iii) Coprecipitation-treated CNF-C@bPEI/HPBA.

Biofilm formation resistance properties of super-hydrophilic gel sensor

Taking into account the high-glucose environment in the oral cavity where the sensor is placed, we conducted further investigations using

metagenomic sequencing to explore the oral bacterial species most influenced by elevated saliva glucose levels. The specific operation protocol is described in Figure S1. *Streptococci*, in particular *S. pneumoniae*, *S. mitis*, and *S. oralis* exhibited the highest increase in relative abundance in the treatment of glucose. Notably, their relative abundance displayed a time- and dose-dependent rise (Figure 4a). Consequently, these strains were selected for evaluating the sensor's anti-biofilm capacity.

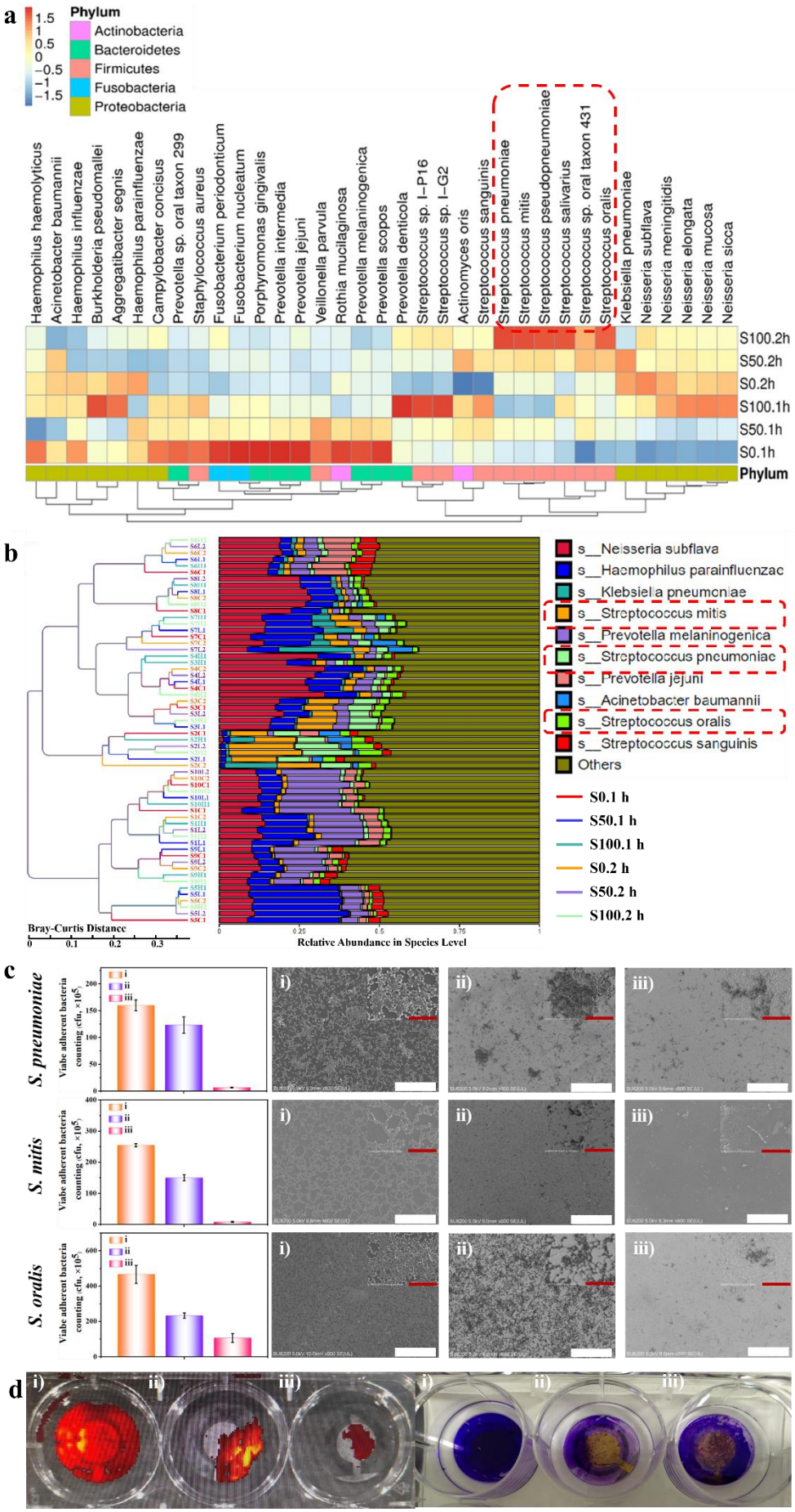
a
Phylum
Actinobacteria
Bacteroidetes
Firmicutes
Fusobacteria
Proteobacteria
Haemophilus haemolyticus
Acinetobacter baumannii
Haemophilus influenzae
Burkholderia pseudomallei
Aggregatibacter segnis
Haemophilus parainfluenzae
Campylobacter concisus
Prevotella sp. oral taxon 299
Staphylococcus aureus
Fusobacterium periodonticum
Fusobacterium nucleatum
Porphyromonas gingivalis
Prevotella intermedia
Prevotella jejuni
Veillonella parvula
Rothia mucilaginosa
Prevotella melaninogenica
Prevotella scopos
Prevotella denticola
Streptococcus sp. I–P16
Streptococcus sp. I–G2
Actinomyces oris
Streptococcus sanguinis
Streptococcus pneumoniae
Streptococcus mitis
Streptococcus pseudopneumoniae
Streptococcus salivarius
Streptococcus sp. oral taxon 431
Streptococcus oralis
Klebsiella pneumoniae
Neisseria subflava
Neisseria meningitidis
Neisseria elongata
Neisseria mucosa
Neisseria sicca
S100.2h
S50.2h
S0.2h
S100.1h
S50.1h
S0.1h
Phylum
b
s__Neisseria subflava
s__Haemophilus parainfluenzae
s__Klebsiella pneumoniae
s__Streptococcus mitis
s__Prevotella melaninogenica
s__Streptococcus pneumoniae
s__Prevotella jejuni
s__Acinetobacter baumannii
s__Streptococcus oralis
s__Streptococcus sanguinis
Others
S0.1 h
S50.1 h
S100.1 h
S0.2 h
S50.2 h
S100.2 h
Bray-Curtis Distance
Relative Abundance in Species Level
c
S. pneumoniae
S. mitis
S. oralis
Viabe adherent bacteria counting, cfu, ×10^5
i)
ii)
iii)
d
i)
ii)
iii)

Figure 4. The relationship between saliva glucose and oral bacteria was analyzed by metagenomic sequencing. a) The inter-species analysis results of bacteria. b) The relative abundance and individual differences of the top 10 bacterial species in total quantity. c) SEM images of the effect of coating on bacteria biofilms: (i) HPBA, (ii) Plasma-treated CNF-C@bPEI/HPBA, and (iii) Coprecipitation-treated CNF-C@bPEI/HPBA. Red scale bar: 10 μm, white scale bar: 50 μm. d) IVIS Spectrum images and crystal violet staining images of the effect of coating on *S. mitis* biofilm: (i) HPBA, (ii) Plasma-treated CNF-C@bPEI/HPBA, and (iii) Coprecipitation-treated CNF-C@bPEI/HPBA.

Subsequently, the biofilm-forming resistance capacity of the different surfaces was evaluated. After 24 h of biofilm formation of *S. pneumoniae*, *S. mitis*, and *S. oralis*, bacteria were counted on the different surfaces. As expected, *S. pneumoniae*, *S. mitis*, and *S. oralis* attached to surface coprecipitation-treated CNF-C@bPEI/HPBA were reduced by 95.8±0.74%, 96.7±0.65%, and 76.8±6.51%, respectively (Figure 4b). This observation was further supported by SEM analysis, which consistently demonstrated a suppression of biofilm formation on the coprecipitation-treated CNF-C@bPEI/HPBA surface.

Given its higher abundance, *S. mitis* was selected for visualization using crystal violet and Filmtracer SYPRO Ruby Biofilm Matrix Stain for staining the biofilm mass and extracellular matrix, respectively. The intensity of crystal violet visually observed and fluorescence detected using the IVIS Spectrum on the coprecipitation-treated coating was remarkable reduced (Figure 4c), providing additional confirmation of its resistance to both bacterial adhesion and extracellular matrix formation in biofilms.

Furthermore, we explored the sensor's adsorption capacity for oral proteins

in Table S4 and Figure S8, which also confirmed the excellent anti-fouling performance of the super-hydrophilic gel sensor.

Saliva glucose detection by super-hydrophilic gel sensors

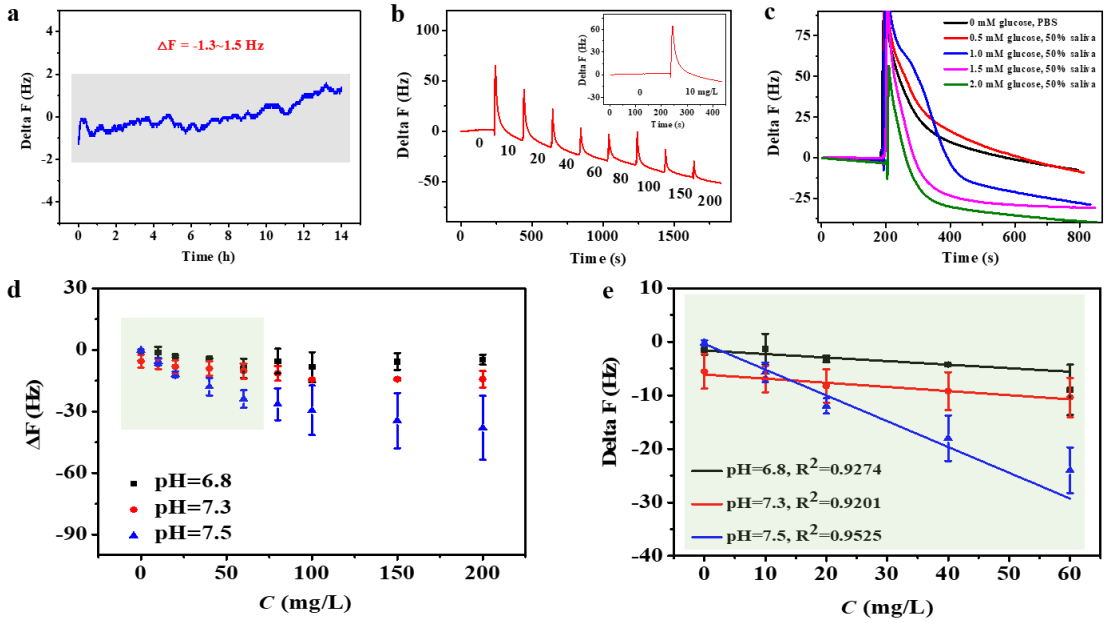

Figure 5. a) Stability test of super-hydrophilic gel QCM sensor. b) Response of the super-hydrophilic sensor to different concentrations of glucose. Inset: response of the superhydrophilic sensor to 0 and 10 mg/L glucose c) Response of the super-hydrophilic sensor to different concentrations of glucose in 50% saliva. d) Response of the super-hydrophilic sensor to different concentrations of glucose at different pH values (6.8–7.5), data are representative of three independent measurements. e) Response trend of the super-hydrophilic sensor to different concentrations of glucose at different pH values (6.8–7.5), data are representative of three independent measurements.

The super-hydrophilic sensor was used to detect saliva glucose, and its sensitivity was evaluated by QCM. First, the ΔF of the Coprecipitation-treated CNF-C@bPEI/HPBA was only between -1.3 and 1.5 Hz within 14 h, indicating the stability of the saliva glucose detection (Figure 5a). Next, different concentrations of glucose were detected in the range of 0~200 mg/L (Figure 5b). The absolute value of ΔF increased rapidly with the rise in glucose concentration, which confirmed the sensor's excellent response

to glucose. In the enlarged plot at the upper right corner of Figure 5b, there was no significant change at baseline when glucose concentration was 0 mg/L. The "baseline" corresponding to the glucose solution gradually decreased, representing that the sensor was constantly adsorbing glucose molecules, rather than the baseline drift. Moreover, as the combination of boric acid and glucose is affected by pH, we tested saliva glucose within the physiological pH range of saliva (Figure 5d). As expected, ΔF increases with increasing pH, because higher pH facilitates the binding of boric acid molecules to glucose molecules in the hydrogel network. In addition, there was a good linear relationship between the concentration of glucose and the response within the range of 0 to 60 mg/L of glucose under different pH conditions (Figure 5e). Moreover, at a pH value of 7.5 and a glucose concentration range of 0 to 60 mg/L, the detection limit was 3.04 mg/L determined by the 3 SD/N method (SD is the standard deviation and N is the slope of linear regression equation). Additionally, with the increase in pH, the corresponding linear correlation coefficients were 0.9274, 0.9201, and 0.9525 at pH values of 6.8, 7.3, and 7.5, respectively.

After that, in order to simulate the low-biocontamination performance of the super-hydrophilic gel sensor in detecting glucose in real saliva samples, we added different concentrations of glucose to 50% saliva (V_{PBS}:V_{Saliva}=1:1) (Figure 5c). The results show an obvious decrease in ΔF with the increase in glucose concentration.

By comparing the detection performance of various saliva glucose sensors in Table S5, the super-hydrophilic gel sensor shows comparable sensitive detection ability of saliva glucose.

Conclusions

In order to address the negative impact of the oral environment on the detection performance of saliva glucose sensors, we have conducted in-depth explorations in the construction of a novel sensor, contributed to the emergence of a super-hydrophilic hydrogel sensor. Endowed with special hydration ability by super-hydrophilic coating on the sensor surface, it exhibits superior resistance to bacterial adhesion and biofilm formation. This feature significantly improves the accuracy of the saliva glucose sensor, with a detection limit of 3.04 mg/L, which met the needs of saliva glucose detection. Therefore, the successful development of the super-hydrophilic gel saliva glucose sensor holds significant importance for fields such as oral health monitoring and management. Additionally, it provides a new approach for the biosensors to improve their reliability and longevity.

Conflicts of interest

There are no conflicts to declare.

Acknowledgements

This work was supported by the National Key R&D Program of China (grant number 2022YFE0118300), the National Key Research and

Development Program of China (grant number 2021YFA1201500), the National Natural Science Foundation of China (grant numbers 51925203 & 32141003), and the Special scientific research project for Capital Hygiene Development focused on the research of “establishment of a mathematical model for saliva glucose and blood glucose, and development of glucose-sensitive anti-fouling nanoprobes” (2022-2-5042), the CAMS Initiative for Innovative Medicine (2021-1-I2M-030, China).

References

[1] M. Dhanya, S. Hegde, Nigerian journal of clinical practice, 19 (2016) 486-490.

[2] Y. Du, W. Zhang, M.L. Wang, Journal of diabetes science and technology, 10 (2016) 1344-1352.

[3] J. Wang, L. Xu, Y. Lu, K. Sheng, W. Liu, C. Chen, Y. Li, B. Dong, H. Song, Analytical Chemistry, 88 (2016) 12346-12353.

[4] R.S. Malon, S. Sadir, M. Balakrishnan, E.P. Córcoles, BioMed research international, 2014 (2014) 962903.

[5] A.C.M. Brito, I.M. Bezerra, M.H.S. Borges, Y.W. Cavalcanti, L.F.D. Almeida, Biofouling, 37 (2021) 615-625.

[6] H. Alqaderi, M. Tavares, M. Hartman, J.M. Goodson, Journal of dental research, 95 (2016) 1387-1393.

[7] W.G. Wade, Periodontology 2000, 86 (2021) 113-122.

[8] N.B. Arweiler, L. Netuschil, Advances in experimental medicine and biology, 902 (2016) 45-60.

[9] J. Xu, H. Lee, Chemosensors, 8 (2020) 66.

[10] P.H. Lin, B.R. Li, The Analyst, 145 (2020) 1110-1120.

[11] N. Liu, Z. Xu, A. Morrin, X.J.A.M. Luo, Analytical methods, 11 (2019) 702-711.

[12] F. Ghilini, D.E. Pissinis, A. Miñán, P.L. Schilardi, C. Diaz, ACS biomaterials

science & engineering, 5 (2019) 4920-4936.

[13] K. Sauer, P. Stoodley, D.M. Goeres, L. Hall-Stoodley, M. Burmølle, P.S. Stewart, T. Bjarnsholt, Nature reviews. Microbiology, 20 (2022) 608-620.

[14] S. Singh, S. Datta, K.B. Narayanan, K.N.J.J.o.G.E. Rajnish, Biotechnology, 19 (2021) 1-19.

[15] D. Chan, J.C. Chien, E. Axpe, L. Blankemeier, S.W. Baker, S. Swaminathan, V.A. Piunova, D.Y. Zubarev, C.L. Maikawa, A.K. Grosskopf, J.L. Mann, H.T. Soh, E.A. Appel, Advanced materials, 34 (2022) e2109764.

[16] N. Wisniewski, M. Reichert, Colloids and surfaces. B, Biointerfaces, 18 (2000) 197-219.

[17] N. Wisniewski, F. Moussy, W.M. Reichert, Fresenius' journal of analytical chemistry, 366 (2000) 611-621.

[18] C.C. Chang, K.W. Kolewe, Y. Li, I. Kosif, B.D. Freeman, K.R. Carter, J.D. Schiffman, T. Emrick, Advanced materials interfaces, 3 (2016) 1500521.

[19] B. Li, P. Jain, J. Ma, J.K. Smith, Z. Yuan, H.C. Hung, Y. He, X. Lin, K. Wu, J. Pfaendtner, S. Jiang, Science advances, 5 (2019) eaaw9562.

[20] Z. Zhu, S. Zheng, S. Peng, Y. Zhao, Y. Tian, Advanced materials, 29 (2017).

[21] S. Chen, L. Li, C. Zhao, J.J.P. Zheng, Polymers, 51 (2010) 5283-5293.

[22] P.J. Molino, D. Yang, M. Penna, K. Miyazawa, B.R. Knowles, S. MacLaughlin, T. Fukuma, I. Yarovsky, M.J.J.A.n. Higgins, ACS nano, 12 (2018) 11610-11624.

[23] X. Liu, J. He, Langmuir : the ACS journal of surfaces and colloids, 25 (2009) 11822-11826.

[24] J. Yang, Z. Zhang, X. Men, X. Xu, X. Zhu, X. Zhou, Q. Xue, Journal of colloid and interface science, 366 (2012) 191-195.

[25] L. Li, Y. Zhang, J. Lei, J. He, R. Lv, N. Li, F. Pan, Chemical communications, 50 (2014) 7416-7419.

[26] J. Fang, A. Kelarakis, L. Estevez, Y. Wang, R. Rodriguez, E.P. Giannelis, Journal of Materials Chemistry, 20 (2010) 1651-1653.

[27] T. Han, Z. Ma, D. Wang, ACS macro letters, 10 (2021) 354-358.

[28] X. An, K. Zhang, Z. Wang, Q.V. Ly, Y. Hu, C. Liu, Journal of Membrane Science,

612 (2020) 118417.
[29] Q. Dou, Z. Zhang, Y. Wang, S. Wang, D. Hu, Z. Zhao, H. Liu, Q. Dai, ACS applied materials & interfaces, 12 (2020) 34190-34197.